NASA CR-166,335

NASA CONTRACTOR REPORT 166335

NASA-CR-166335
19820020375

VISCOUS EFFECT ON AIRFOILS FOR UNSTEADY TRANSONIC FLOWS

Shen C. Lee

University of Missouri - Rolla

Consortium Agreement No. NCA2-OR450-001
June 1982

NASA

NASA CONTRACTOR REPORT 166335

VISCOUS EFFECT ON AIRFOILS FOR UNSTEADY TRANSONIC FLOWS

Shen C. Lee

University of Missouri - Rolla
Rolla, Missouri 65401

Prepared for
Ames Research Center
under Consortium Agreement
No. NCA2-OR450-001

National Aeronautics and
Space Administration

Ames Research Center
Moffett Field, California 94035

TABLE OF CONTENTS

NOMENCLATURE

A	Coefficient of ϕ_{tt} for equation (1)
B	Coefficient of ϕ_{xt} for equation (1)
C	Coefficient of ϕ_{xx} for equation (1)
C_p	Pressure coefficient
c	Airfoil chord length
f_{xm}	Slope of the modified airfoil
f_{xo}	Slope of the original airfoil
H	Shape factor
I	Number of iteration
i	Number of iterations before I
K	Dimensionless frequency
M	Mach number
m	Exponent of coefficient C
N	Transformed coordinate of n
N_{sp}	Number of supersonic points
n	Coordinate normal to the surface
P	Pressure
R	Residual of each iteration
Re	Reynolds number
S	Transformed coordinate of s
s	Coordinate along the surface
T	Temperature
t	Time
U	Transformed velocity of u
U_∞	Free stream velocity
u	Velocity component in the s-direction

v	Velocity component in the n-direction
$v(s)$	Surface vertical velocity
w	Wedge thickness
x	Physical coordinate in the flow direction
y	Physical coordinate normal to x
α	Angle of attack
β_1	Coefficient for wedge thickness
β_2	Coefficient for vertical surface velocity
γ	Specific heat ratio
δ	Airfoil thickness to chord ratio
δ_{tr}	Transformed boundary layer thickness
δ^*	Displacement thickness
θ	Momentum thickness
θ_{max}	Maximum wedge angle
ν	Kinematic viscosity
ρ	Density
τ	Shear stress
ϕ	Velocity potential
ω	Frequency

Subscript

acpt	Acceptable value
e	Edge of the boundary layer
i	Adiabatic condition
max	Maximum value
n	Derivative with respect to n
ref	Reference point

s Derivative with respect to s

sh Shock location

t Derivative with respect to time

tr Transformed parameter

w Wall

x Derivative with respect to x

y Derivative with respect to y

o Stagnation

1 Upstream of the shock wave

∞ Free stream

Superscript

- Temperature averaged parameter

I. INTRODUCTION

Experimental work by Spaid and Bachalo (1) using holographic interferometry produced some clear pictures of the density distribution for transonic flow about airfoils. It clearly indicates that there are regions in which the viscous effect plays an important role:

1. The shock/boundary-layer intereaction region.
2. The boundary layer development region.
3. The wake region.

In order to predict aerodynamic performances, it is desirable to solve the time dependent Navier-Stokes equations as illustrated by Lin et al. (2) for low Reynolds number flows. However, the current generation of high speed computers has not yet reached the computational speed for this approach to be realistic for analyzing transonic flows, as discussed by Chapman (3). Steger (4) solved the Reynolds equations for transonic flows with a substantial computation time, using a simple closure scheme for turbulent stresses. With advancing computer design and improving turbulence modeling, this method has a high potential to be the design tool in the near future. However, for practical applications, it is still necessary to use viscous correction of an inviscid solution for which many efficient computational methods (5,6, and 7) have been developed.

Several approaches are available to consider the viscous effect for inviscid analysis. Yoshihara and Zonar (8) used an empirical model of viscous ramp to approximate the suddenly thickened boundary layer behind a shock wave. It requires the least amount of computation if the contour of the ramp can be adjusted so that it will converge to the inviscid solution. However, the boundary layer effect before the ramp is totally ignored. Nash and Scruggs (9) solved the differential boundary layer equation for velocity distributions in the boundary layer region. However, the sudden pressure increase behind a shock could not be adequately treated. Consequently, it becomes very inefficient in determining the actual shock location, especially when flow separation appears possible. Green, et al. (10) developed a lag-entrainment method to solve the integral boundary layer equation together with the lag-entrainment equations for the displacement thickness. Collyer and Lock (11) and Melnik, et al. (12) applied this method to the inviscid code developed by Jameson (13 and 14) and obtained some results that agreed with experimental data. However, the Green's lag-entrainment method required a large number of empirical constants which have not been physically verified. Moreover, the computational time required for the viscous correction made the computational efficiency of the inviscid code irrelevant.

The objective of this study is to develop a viscous correction method which not only improves the accuracy of the inviscid solution but also maintains its computational efficiency. A viscous ramp (8), can be used to partially simulate the suddenly thickened boundary layer behind a shock wave. An available method of solving the integral boundary layer equation can be used to calculate the displacement thickness. It is noted that a conventional integral boundary layer method modifies the sudden increase of pressure behind a shock by a lesser pressure gradient with a longer distance. Inserting a viscous wedge at the foot of the shock can correct this

situation, if the empirical relation for wedge thickness is designed to supplement the inadequancy of the boundary layer method. The inviscid correction before the shock can be adequately obtained by a conventional boundary layer method. The viscous correction behind the shock is accomplished by superpositioning the viscous wedge thickness on the displacement thickness. For a strong shock situation, the empirical relation of the viscous wedge may include the existence of a separation bubble. Lee and Van Dalsem (15) developed a viscous correction method for the inviscid full-potential code, TAIR (16). By comparing with experimental data, it gives similar results as other correction methods by improving the accuracy of the inviscid solution for moderately strong shock situations. However, contrary to other correction methods, it reduces the computational time by reducing the numbers of iteration for reaching a converged solution. The improved computational efficiency makes this method more attractive in correcting inviscid solutions for unsteady state maneuvering as well as for three-dimensional wings.

Inviscid solution for airfoils maneuvering at low frequency unsteady motions was obtained by Ballhaus and Goorjian (17). Rizzetta and Yoshihara (18) used an order of magnitude analysis to show that the turbulent boundary layer of an airfoil reaches steady state during low frequency maneuvering. However, the computational time becomes a critical factor for practical applications. Owing to the improvement both in accuracy and in computational time, this study is to apply the same principle of the viscous wedge and the conventional boundary layer for viscous correction of an inviscid small disturbances code, LTRAN2 (19).

II. LTRAN2

The equation of motion for an unsteady two-dimensional, transonic flow with small disturbance assumption, according to Landahl (20), may be written as:

$$A\phi_{tt} + 2B\phi_{xt} = C\phi_{xx} + \phi_{yy} \tag{1}$$

with

$$A = K^2 M_\infty{}^2/\delta^{2/3}$$

$$B = K\, M_\infty{}^2/\delta^{2/3}$$

$$C = (1-M_\infty{}^2)/\delta^{2/3} - (\gamma + 1)M_\infty{}^m\, \phi_x$$

Where ϕ is the disturbance velocity potential, M_∞ is the free-stream Mach number, γ is the ratio of specific heats, and δ is the airfoil thickness-to-chord ratio. The subscripts x,y, and t are the independent variables of space and time. The quantities x, y, t and ϕ in equation (1) have been scaled by c, $c/\delta^{1/3}$, ω^{-1}. amd $c\delta^{2/3}U_\infty$, respectively. For an airfoil of chord length c, traveling with a velocity U_∞, and executing some unsteady oscillatory motion of frequency ω, the reduced frequency K is defined as:

$$K = \omega c/U_\infty \tag{2}$$

The choice of the exponent m for the coefficient C is somewhat arbirary and is taken to be 2 using the Spreiter scaling. At low reduced

frequencies, equation (1) can be approximated as:

$$2B\phi_{xt} = C\phi_{xx} + \phi_{yy} \tag{3}$$

which can be obtained from the Euler's equation by assuming

$$K \sim \delta^{2/3} \sim 1 - M_\infty << 1 \tag{4}$$

Solutions of equation (3) were obtained using LTRAN2 which was developed by Ballhaus and Goorjian (17) for $K < 0.2$ and modified by Hessenius and Goorjian (19) for $K < 1.0$ with the pressure coefficient defined as:

$$Cp = -2(\phi_x + K\phi_t) \tag{5}$$

LTRAN2 uses an H-grid which reasonally satisfies the orthogonality condition around the airfoil and in the wake region. Using an alternating directional implicit (ADI) algorithm and an approximate factorization (AF2) scheme, both steady and unsteady solutions can be obtained with reasonable computational time for relatively thin airfoils. Consideration of viscous corrections needs not only to improve the accuracy but also to maintain the computational speed.

III. SHOCK/BOUNDARY-LAYER INTERACTION

The occurence of a shock wave not only causes a discontinuity in the inviscid flow region but also produces a stronger adverse pressure gradient in the boundary layer region. Downstream of a shock wave, the boundary layer is suddenly thickened. Sometimes, it may be accompanied by a region of flow separation. Theoretically only the Reynolds equations, which are obtained from the time averaged Navier-Stokes equations, are adequate in analyzing the phenomenon of shock/boundary layer interaction (4). However, the required computer time for such a small region makes it impractical for industrial applications. Yoshihara and Zonars (8) used a viscous ramp to approximate the suddenly thickened boundary layer region behind a shock wave with reasonable success. Lee and Van Dalsem (15) developed a method by using a simpler viscous wedge superimposed on a turbulent boundary layer for correcting steady full-potential solutions. The same principle is being applied for unsteady small disturbance solution as follows:

A. Viscous Wedge

An empirical formula, which simulates the suddenly thickened boundary layer behind the shock, was developed by Lee and Van Dalsem (15) and is used here as follows:

$$\frac{w}{c} = \begin{cases} 0, & \text{for } s < s_{sh} \\ \beta_1 \theta_{max} \left\{ 1 - \exp\left[(s_{sh} - s)/c\beta_1 \right] \right\}, & s \geq s_{sh} \end{cases} \tag{6}$$

where β_1 is an empirical constant ($\beta_1 = 0.1$ has been used for both

full-potential and small disturbance corrections). θ_{max} is the maximum deflection angle for an attached shock at a given upstream Mach number, M_1, which is determined by the inviscid code. s is the distance along the surface of the airfoil with s_{sh} as the location of the shock wave. For thin airfoils, the suddenly thickened boundary layer can be treated as an equivalent vertical surface velocity, v; which is used as a boundary condition for the inviscid flow solver.

$$v(s) = \beta_2 [M(s) \cdot w(s)]_s \tag{7}$$

where β_2 is an empirical constant ($\beta_2 = 2$ for the unsteady small disturbance correction). The vertical surface velocity needs to be scaled by δ in order to be treated similarly as other parameters resulted in surface variations during unsteady motions. The required additional computing time for evaluating the wedge thickness, w, and the vertical surface velocity, v, is negligible.

B. Boundary Layer

Boundary layer always develops before the shock wave. Near the leading edge, there is a laminar boundary layer region which is followed by a transition region and a turbulent region. In transonic flow, the laminar and the transition regions are very small, their effect to aerodynamic performance is insignificant. A simple method given by Cohen and Roshtko (21) was used mainly to provide the initial condition for the turbulent boundary layer. Assuming that transition occurs instantaneously at a prescribed location, an integral method for turbulent boundary layer developed by Sasman and Cresci (22) was used. The time-averaged continuity and momentum equations for two-dimensional, steady, compressible, turbulent flow can be expressed as:

$$(\rho u)_s + (\rho v)_n = 0 \tag{8}$$

$$\rho u(u)_s + \rho v(u)_n = -(P)_s + (\tau)_n \tag{9}$$

where u and v are the velocity components in the s and n directions, respectively, and τ is the shear stress. Since the temperature variation in the boundary layer is significant at transonic speeds, the Mager transformation (23) is employed to simplify the integral equation. The transformed coordinates are:

$$S = \int_0^s \left(\frac{T_o}{\bar{T}}\right) \left(\frac{T_e}{T_o}\right)^{(\gamma+1)/[2(\gamma-1)]} ds \tag{10}$$

$$N = \left(\frac{T_e}{\bar{T}_o}\right)^{1/2} \int_0^n \frac{\rho}{\rho_o} dn \tag{11}$$

T_e is a function of s; $\bar{T}$ is the reference temperature,

$$\frac{\overline{T}}{T_o} = 0.5\,\frac{T_w}{T_o} + 0.22\,Pr^{1/3} + (0.5 - 0.22\,Pr^{1/3})\left(\frac{T_e}{T_o}\right) \tag{12}$$

where Pr is the Prandtl number. The shape factor, H, and the momentum thickness, θ, are related to the transformed shape factor, H_{tr}, and the transformed momentum thickness, θ_{tr}, as follows:

$$H = \frac{T_w}{T_o}\left[1 + \frac{\gamma - 1}{2}\,Me^2\right]\,H_{tr} + \frac{\gamma - 1}{2}\,Me^2 \tag{13}$$

$$\theta = \left[\frac{T_o}{T_e}\right]^{(\gamma+1)/[2(\gamma-1)]}\theta_{tr} \tag{14}$$

with

$$H = \frac{\delta^*}{\theta} \tag{15}$$

where M_e is the Mach number at the edge of the boundary layer. The displacement thickness, δ^*, may then be expressed

$$\delta^* = (\theta_{tr} + \delta^*_{tr})\left(\frac{T_o}{T_e}\right)^{(3\gamma-1)/[2(\gamma-1)]} - \theta_{tr}\left(\frac{T_o}{T_e}\right)^{(\gamma+1)/[2(\gamma-1)]} \tag{16}$$

For adabatic flow, the transformed displacement thickness, δ^*_{tr}, and the transformed momentum thickness, θ_{tr}, are defined as

$$\delta^*_{tr} = \int_o^{\delta_{tr}}\left(1 - \frac{U}{U_e}\right)dN \tag{17}$$

$$\theta_{tr} = \int_o^{\delta_{tr}}\frac{U}{U_e}\left(1 - \frac{U}{U_e}\right)dN \tag{18}$$

where δ_{tr} is the boundary-layer thickness in the transformed coordinates, and U is the transformed velocity component in the s direction, with

$$U = u\left(\frac{T_o}{T_e}\right)^{1/2} \tag{19}$$

The transformed velocity profile in the turbulent boundary layer obeys the power law:

$$\frac{U}{U_e} = \left(\frac{N}{\delta_{tr}}\right)^{[(H_{tr})_i - 1]/2} \tag{20}$$

where the adabatic shape factor $(H_{tr})_i$ is defined as

$$(H_{tr})_i = \frac{\delta^*_{tr}}{\theta_{tr}} \tag{21}$$

The transformed mementum integral equation can be written as

$$\frac{d\theta_{tr}}{dS} + \frac{\theta_{tr}}{U_e}\frac{dU_e}{dS}\left[2 + \frac{T_w}{T_o}(H_{tr})_i\right] = \left(\frac{T_o}{T_e}\right)^{0.268}\left(\frac{\bar{T}}{T_o}\right)^{1.268}\frac{\tau_w}{\rho_e U_e^2} \tag{22}$$

The transformed moment-of-momentum equation the becomes

$$\frac{d(H_{tr})_i}{dS} = -\frac{1}{2U_e}\frac{dU_e}{dS}(H_{tr_i})[(H_{tr})_i + 1]^2[(H_{tr})_i - 1]\left[1 + \left(\frac{T_w}{T_o} - 1\right)\frac{(H_{tr})_i^2 + 4(H_{tr})_i - 1}{[(H_{tr})_i + 1][(H_{tr})_1 + 3]}\right] + \frac{[(H_{tr})_i^2 - 1]}{\theta_{tr}}\left(\frac{\bar{T}}{T_e}\right)\left[\frac{(H_{tr})_i\,\tau_w}{\rho_e U_e^2} - \frac{[(H_{tr})_1 + 1]\tau_w}{\rho_e U_e^2}\int_o^1 \frac{\tau}{\tau_w}\,d\left(\frac{N}{\delta_{tr}}\right)\right] \tag{23}$$

The shear stress at the wall, τ_w, is expressed through an empirical relation given by Tetervin (24) as

$$\tau_w = 0.123\,\rho_e U_e^2\left(\frac{U_e\theta_{tr}}{\bar{\nu}}\right)^{-0.268}\left(\frac{T_e}{\bar{T}}\right)^{1.268} e^{-1.561(H_{tr})_1} \tag{24}$$

where $\bar{\nu}$ is the kinematic viscosity at temperature $\bar{T}$. The two ordinary differential equations, Equations (22) and (23), can be solved simultaneously using the 4th order Runge-Kutta method for the shape factor, H, and the momentum thickness, θ.

A computer code, BLAYER, which was developed by McNally (25), gives the solutions of the displacement thickness, δ^*, for both the laminar and the

turbulent regions. Before the shock wave, the displacement thickness is the only source for the vertical component of the surface velocity. After the shock wave, the summation of the displacement thickness and the wedge thickness becomes the source of the vertical component of the surface velocity, v.

$$v(s) = \beta_2 \left\{ M(s) \left[w(s) + \delta^*(s) \right] \right\}_s \tag{25}$$

The integral boundary layer method solves two simultaneous ordinary differential equations using relatively small amount of computational time. Nevertheless, it is about two orders of magnitude longer than that of the viscous wedge.

C. Wake

The wake region affects the transonic aerodynamic performance only in the vicinity of the trailing edge. Its contribution to drag force can be substantial, expecially when separation occurs before the trailing edge. Accurate evaluation of the wake region needs to include the possibility of flow separation which requires the solution of the Reynolds equations. For the interest of industrial application, the constraint of computational time calls for a simpler approach. Since the viscous wedge is capable of approximating the separation region before the trailing edge, it is advantageous to terminate the boundary layer analysis earlier by using a lower value shape factor for flow separation. $H = 1.8$ was used in this study. The wake is then considered as an extended airfoil with its effective thickness determined as follows:

i) If no flow separation occurs along the airfoil, the summation of the displacement thickness and the wedge thickness is assumed constant from the trailing edge throughout the wake.

ii) If flow separation occurs along the airfoil, the summation of the displacement thickness, the wedge thickness and the airfoil thickness at the point of separation is assumed constant from the separation point throughout the wake.

IV. METHOD OF SOLUTIONS

The objective is to consider the viscous effect without substantially increasing computational time. It is desirable that the basic algorithm of LTRAN2 be modified only when the viscous effect can make a meaningful contribution. The flow chart in Figure 1 shows both the inviscid and the viscous solutions for the steady and unsteady calculations. Figure 1a consists of the input information and the grid generation for LTRAN2. The H-grid, once generated, remains unchanged for both steady and unsteady calculations. Two possible methods can be used for steady state solutions. The standard method, as shown in Figure 1b, is an iterative procedure known as AF2 to solve the steady state equations. The alternative method, as shown in Figure 1c, solves the unsteady equations with the steady state boundary condition. The alternative method allows the time interval be chosen as small as necessary to obtain a converged solution. Once the steady state solution is known,

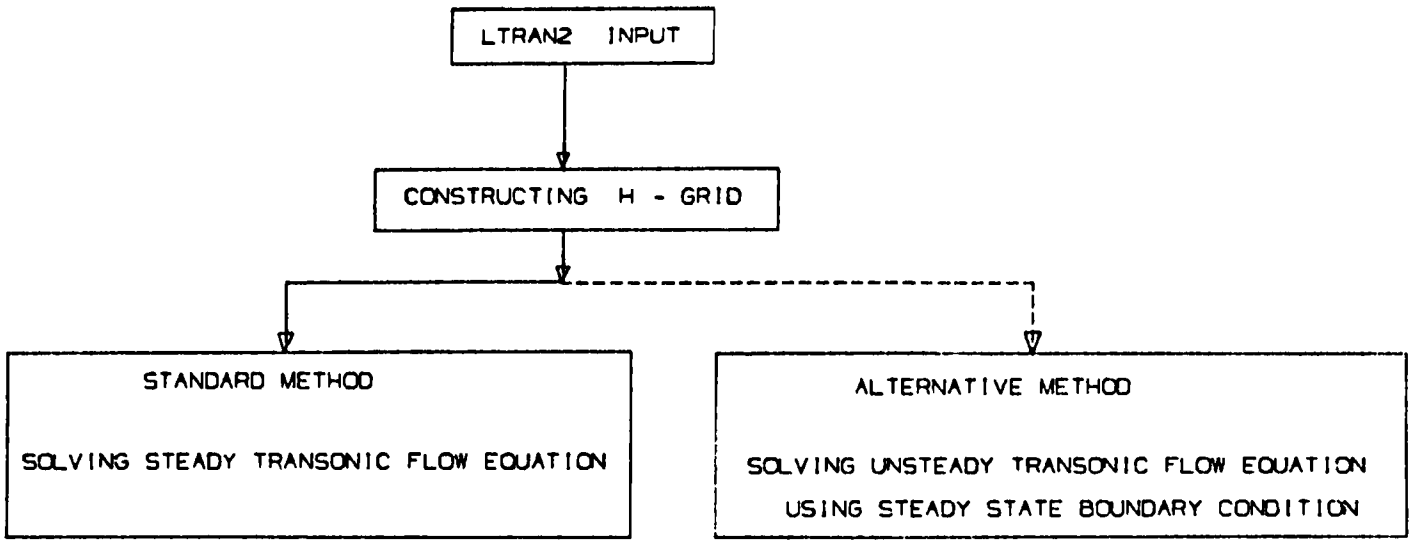

FIGURE 1A. FLOW CHART FOR GRID CONSTRUCTION OF LTRAN2

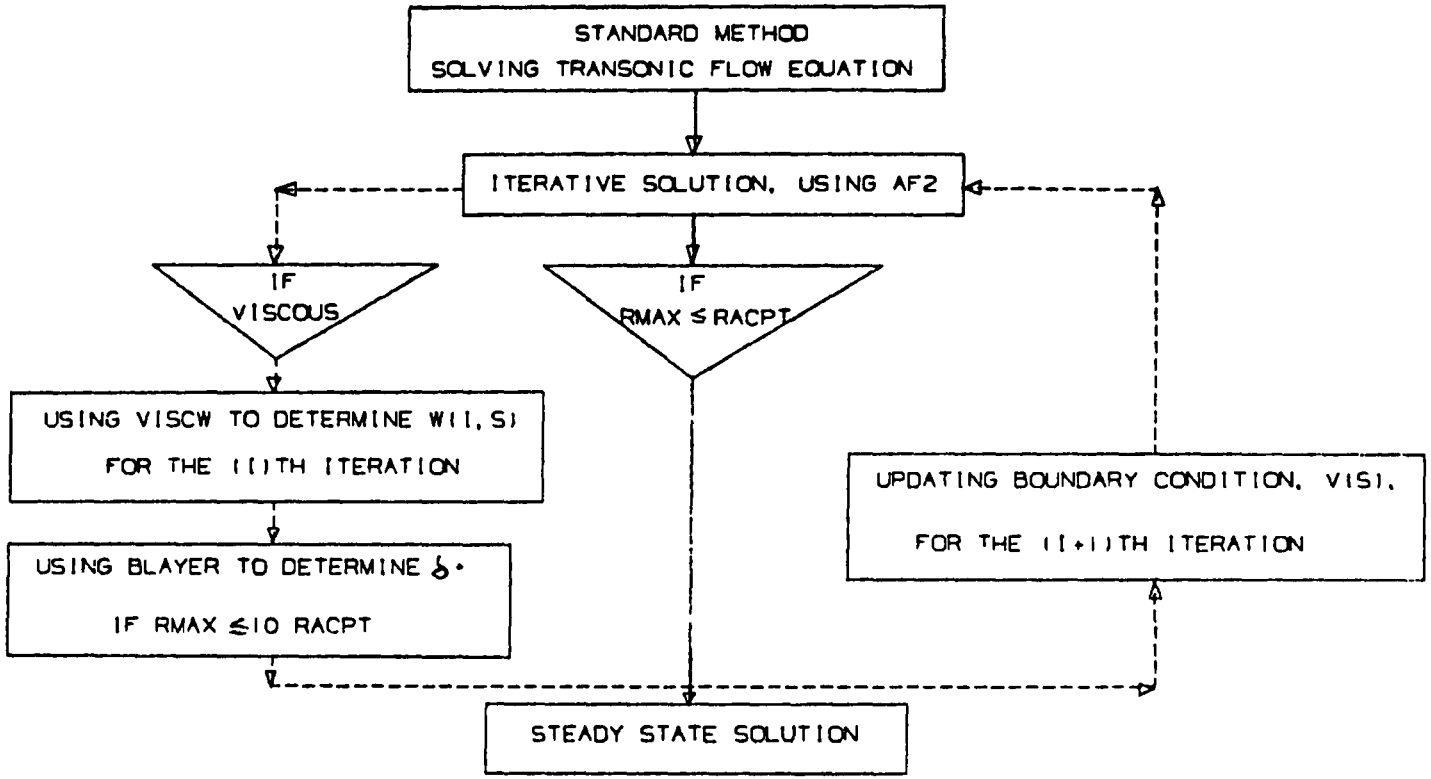

FIGURE 18. FLOW CHART FOR THE STANDARD METHOD TO OBTAIN STEADY STATE SOLUTION

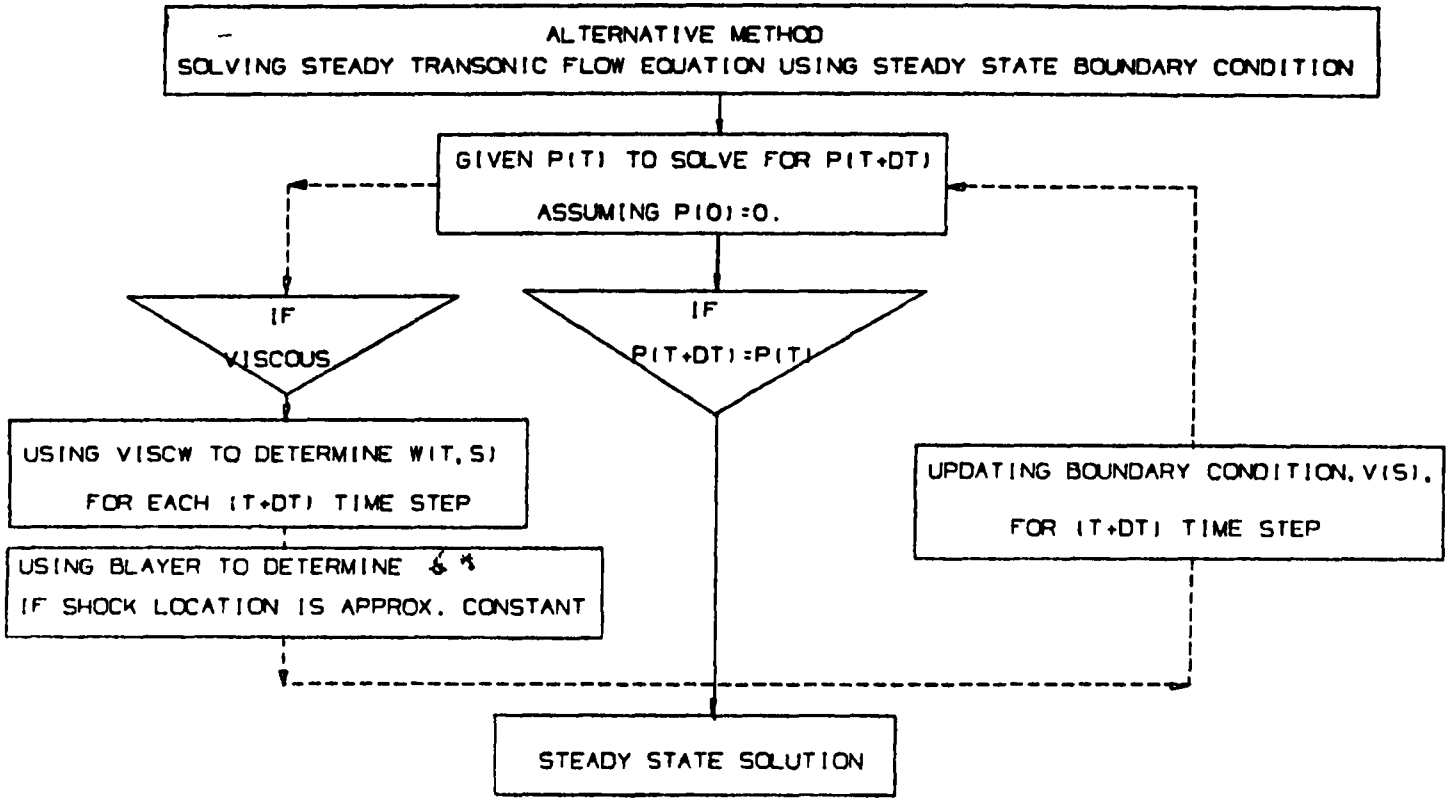

FIGURE 1C. FLOW CHART FOR THE ALTERNATIVE METHOD TO OBTAIN STEADY STATE SOLUTION

Figure 1d shows that the unsteady calculations can be conducted by prescribing a given function of time for the unsteady motions.

The viscous correction consists of two major components: the viscous wedge, VISCW, and the boundary layer, BLAYER. This section outlines the logic and the procedures of the viscous correction.

A. Logic For Viscous Correction

The pressure coefficient is closely related to the shock location which is sensitive to the viscous wedge approximation. However, the abrupt change of the airfoil surface due to the wedge insertion, especially at higher upstream Mach numbers, causes instability for the numerical method. On the other hand, the boundary layer displacement thickness before the shock wave does not have any significant variations during low frequency unsteady motions. Since the computational time required for the wedge thickness is approximately 1% of that for the boundary layer development, it is necessary to use a minimum number of corrections by the boundary layer method. It appears logical to divid the viscous effect into two portions:

i) The Boundary Layer Portion

The boundary layer displacement thickness, which is relatively insensitive to the frequency maneuvering, can be calculated by a conventional integral boundary layer method. It provides the following functions:

a) The viscous effect, that exists between the leading edge and the shock wave, gives a more realistic Mach number upstream of the shock.
b) A smooth transition for the airfoil contour at the foot of the shock can eliminate the need of a precursor for the viscous ramp used by Yoshihara and Zonar (8).
c) An effective wake thickness can be calculated throughout the wake region.

ii) The Wedge Portion

The viscous wedge thickness, which is responsible to the change of shock locations at every instant of the low frequency maneuvering, needs to be used to complement the boundary layer results as follows:

a) The suddenly thickened boundary layer behind a shock can be simulated.
b) The possibility of a separation bubble can be included in the wedge thickness.
c) The wake region.can be reasonably approximated even if separation occurs before the trailing edge.

B. Procedures

Table 1 gives a list of parameters used for the viscous correction of LTRAN2. Both the wedge thickness, w, and the boundary layer displacement thickness, δ^* are a function of the distance, s, along the airfoil surface in the flow direction, x. Different procedures are used for steady and unsteady states.

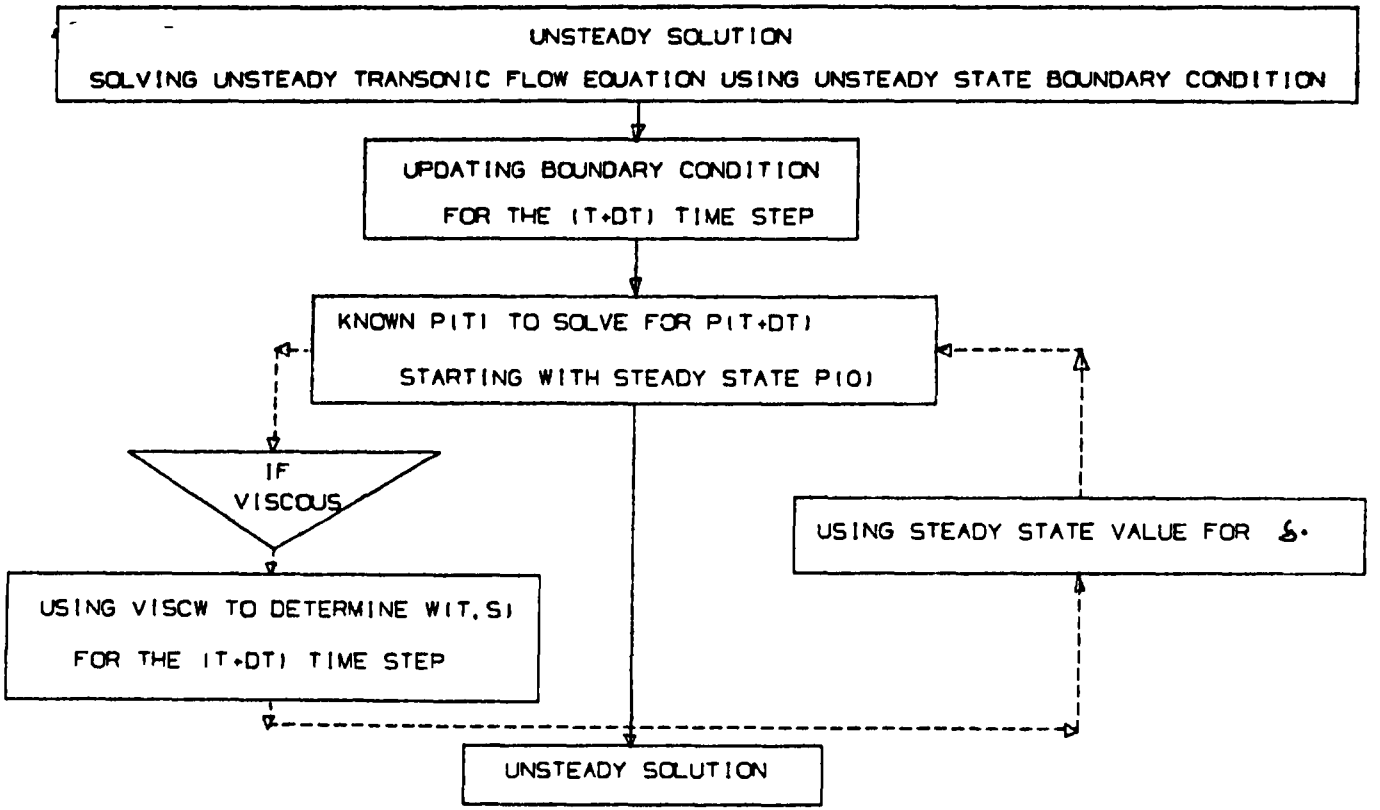

FIGURE 10. FLOW CHART FOR OBTAINING UNSTEADY SOLUTION

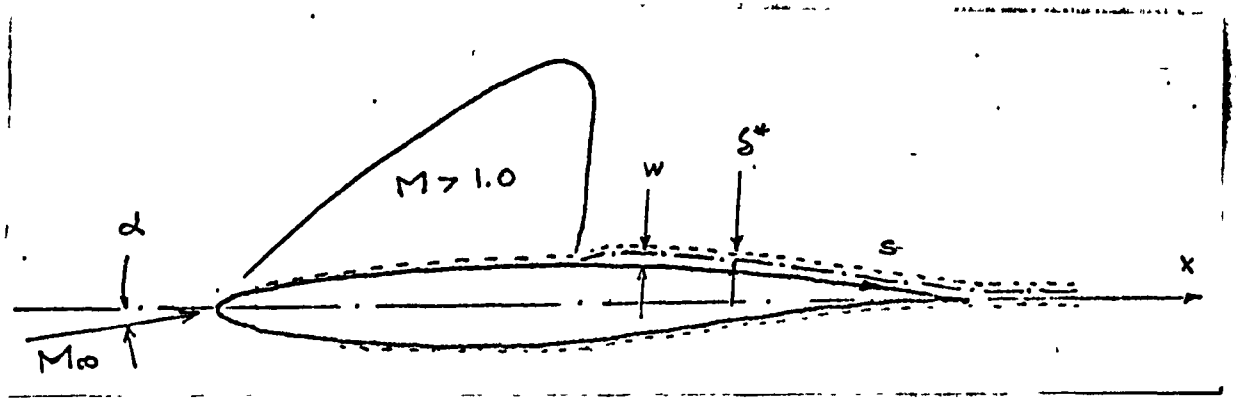

	PARAMETERS	CONDITION
STEADY STATE, T=0. (I)TH ITERATION	W(I, S)	NSP(I) = NSP(I-6+ i), i = 1, 2, ..., 6
	•(S)	RMAX ≤ 10 RACPT
	W(I, S) = W(I-1, S)	RMAX ≤ 5 RACPT
	$V(S) = \frac{\beta_2}{\delta}\left[M\ (W(I, S) + \delta^*(S))\right]_S$	RMAX ≤ RACPT
UNSTEADY STATE (T)TH TIME STEP	W(T, S)	
	$V(T, S) = \frac{\beta_2}{\delta}\left[M\ (W(T, S) + \delta^*(S))\right]_S$	

TABLE I. VISCOUS CORRECTION PARAMETERS

i) Steady Calculations

Assuming the vertical component of the surface velocity is zero, the steady calculation for the standard method can be started the same way as the inviscid solution. At the (I)th iteration, the wedge thickness, w(I,s), can be calculated using Equation (6) when the number of supersonic points, NSP(I), remains constant for six consecutive iterations. The boundary condition of the inviscid flow solver is then modified by Equation (7) for every iteration. The maximum residual, R_{max}, is monitored to compare with an acceptable residual, R_{acpt}, which is prescribed. The boundary layer displacement thickness, $\delta^*(s)$ will be evaluated only once when $R_{max} \leq 10\ R_{acpt}$. The boundary condition of the inviscid flow solver is then modified by Equation (25). The values of $\delta^*(s)$ encounters no significant changes between the leading edge and the shock location as R_{max} approaches to R_{acpt}. Since the boundary layer variation behind the shock is contributed mainly by the viscous wedge, the wedge thickness, w(I,s), will be recalculated at every iteration and is superimposed on the available $\delta^*(s)$. When $R_{max} \leq 5\ R_{acpt}$, the wedge thickness is "frozen" so that w(I,s) = w(I-1,s) until $R_{max} \leq R_{acpt}$. The converged steady state solution for viscous correction is then obtained.

Evaluation of this procedure was conducted by comparing with experimental data as well as with the inviscid solution. The viscous correction, generally, gives better agreement with the experimental data and uses less numbers of iteration than the inviscid solution for moderately strong shock situations. However, there were cases that the standard method failed to converge. An alternative method using a smaller time interval allows the unsteady procedure to be used for steady calculations. This will be discussed in the following section.

ii) Unsteady Calculations

At a given time, t, the wedge thickness w(t,s) can be calculated using Equation (6). Superimposing on the steady state displacement thickness, $\delta^*(s)$, the boundary condition of the inviscid flow solver can be determined using Equation (25). It is assumed that the low frequency unsteady motion does not have any significant effect on the boundary layer development from the leading edge to the shock location. The sacrifice in accuracy for the pressure coefficient was found to be insignificant but the savings in computer time was substantial. In case that the alternative method was used for steady state solutions, the wedge thickness was superimposed on the boundary layer thickness which was evaluated at a prescribed time step where an approximated steady state shock position was established.

V RESULTS AND DISCUSSIONS

Both conventional and supercritical airfoils were studied. Thin airfoils, such as NACA64A010, can be analyzed using LTRAN2 with reasonable accuracy and will not be discussed here. This section considers two supercritical airfoils, RAE 2822 and NLR 7301. Their cross-sections are given in Figure 2.

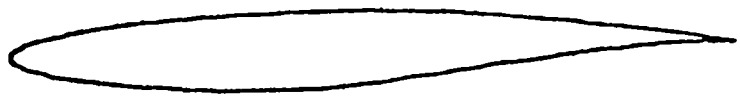

RAE 2822 AIRFOIL

NLR 7301 AIRFOIL

Figure 2, Investigated Airfoils

A. RAE 2822 Airfoil

The geometry and some experimental data were given by Cook et. al., (26). The RAE 2822 airfoil has a maximum thickness to chord ratio of 0.1210. The case of $M_\infty = 0.73$, $\alpha = 3.19$, $Re_\infty = 6.5 \times 10^6$ oscillating 1 degree about $x/c = 0.5$ at a reduced frequency $K = 0.2$ was studied.

i) Steady State Solution

Due to the large angle of attack, the alternative method of using the unsteady state procedure with very small time increment was adopted. Converged steady state solutions were obtained at the 2010th iteration, which corresponds to a dimensionless time of 17.54, for both the inviscid and the viscous solutions. The boundary layer was calculated at the 510th iteration where the shock wave approached its final position. Figure 3 shows the Mach number distributions. It is noted that the viscous solution gives a slightly lower Mach number before the shock. This is due to the boundary layer effect from the leading edge to the shock location. The combined effect of the viscous wedge and the boundary layer moves the shock closer to the leading edge than the inviscid solution. Figure 4 shows the pressure coefficient distributions. The viscous correction gives the shock location at $x/c = 0.49$, while the inviscid solution is at $x/c = 0.63$ in comparison with the experimental data at $x/c = 0.53$. The viscous correction gives better agreement with the experimetal data. Nevertheless, it over-corrects the shock location. Examining the results of Rizzeta (27) which used the combination of the viscous ramp (8) and the Green's lag-entrainment boundary layer method (10), the shock location was at $x/c = 0.39$, an even higher over-correction than the present method.

ii) Unsteady State Solution

Once the steady state solution is reached. The airfoil is forced to execute a pitching motion about the midchord, $x/c = 0.5$, with a reduced frequency $K = 0.2$ at an amplitude of $\alpha_1 = 1.0$ degree. The instantaneous angle of attack, α, is given as a function of time, t, as follows:

$$\alpha = \alpha_o + \alpha_1 \sin(t) \qquad (26)$$

where $\alpha_o = 3.19$ is the steady state angle of attack. Figure 5 shows the comparison between inviscid and viscous solutions at $\alpha = 4.18$ degrees or $t = 39.41$. Figure 6 shows the same comparison at $\alpha = 2.35$ degrees or $t = 48.12$. The viscous effect on the magnitude of the pressure coefficient before the shock is relatively small. The effect on shock location is significant. To evaluate the unsteady results, the magnitude of the pressure coefficient and the phase angle were integrated between the 4th and 5th cycles. Figures 7 and 8 show the magnitude of the integrated pressure coefficient and the phase angle, respectively. The viscous effect reduced the maximum magnitude from 45.5 at $x/c = 0.67$ to 27.8 at $x/c = 0.58$ and the phase angle changed from 106/-86 degrees at $x/c = 0.77$ to 130/-70 degrees at $x/c = 0.64$. The inviscid solution took 40.32 min. CPU time and the viscous solution took 40.52 min. CPU time on the AMDHAL 470/v7 computer. It is evident that the alternative method for viscous correction improves the accuracy of the inviscid solution without any substantial increase of computational time. Moreover, in comparison with the more time consuming lag-entrainment method, the conventional integral boundary layer method is quite adequate if a simple empirical viscous wedge model is being used.

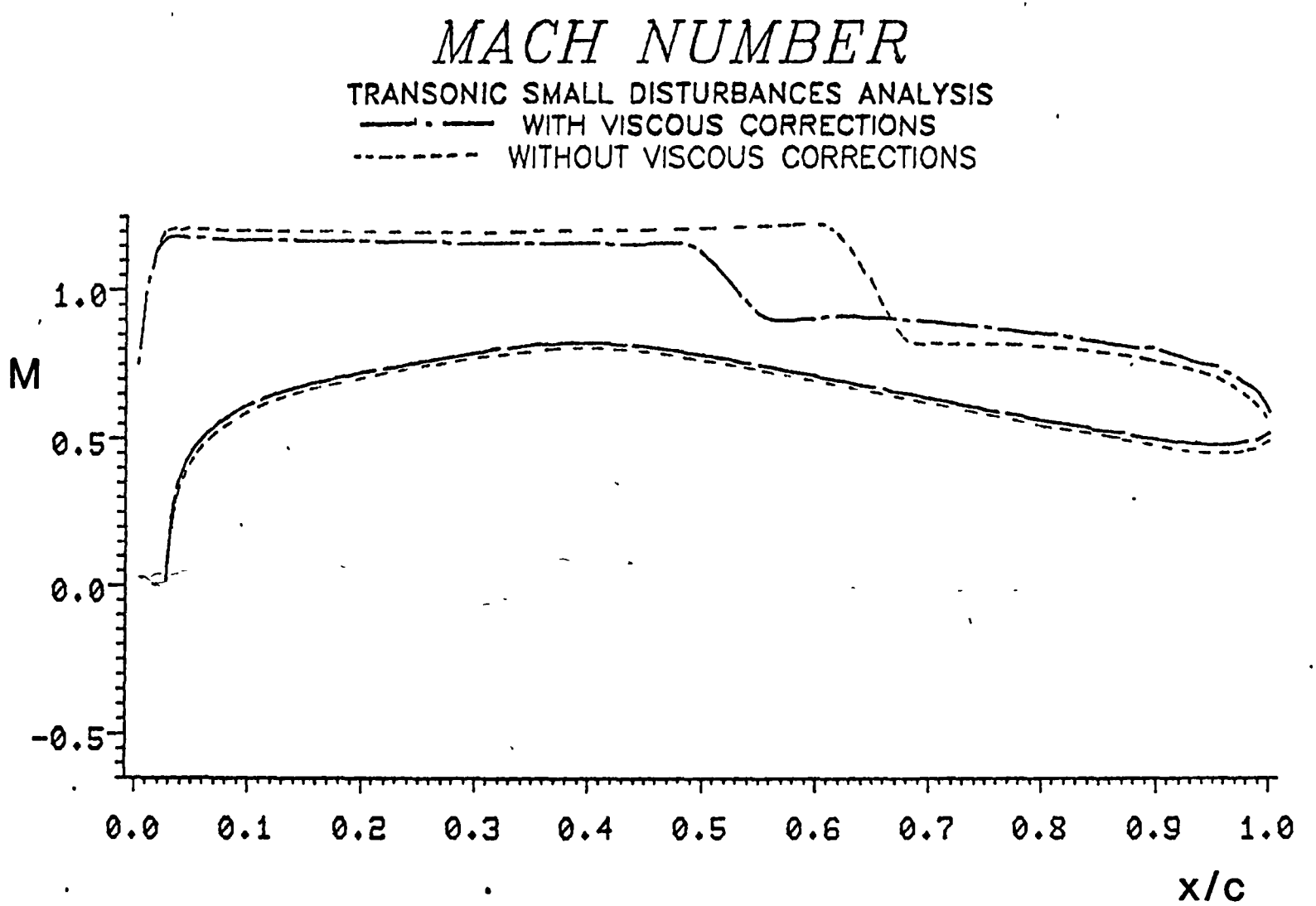

Figure 3, Mach Number Distribution (RAE 2822)

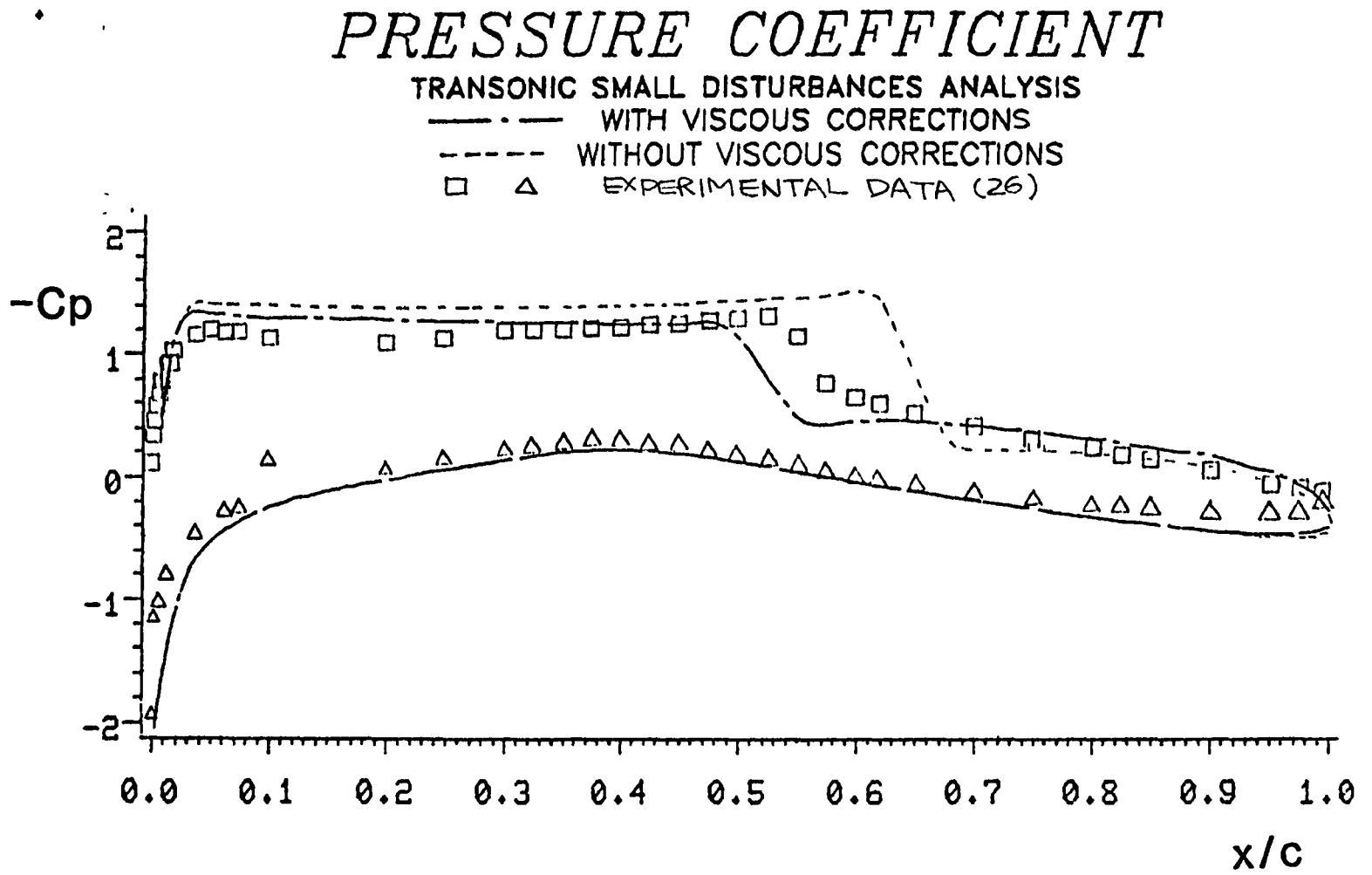

RAE 2822 AIRFOIL MINF=0.730 ALF=3.19
UNSTEADY STATE T=0.0, ALF=3.19DEG.
OSCILLATING 1.0 DEG. WITH K=0.2 AT X/C=0.5
UNSTEADY PROCEDURE FOR STEADY SOLUTION

Figure 4, Pressure Distribution (RAE 2822)

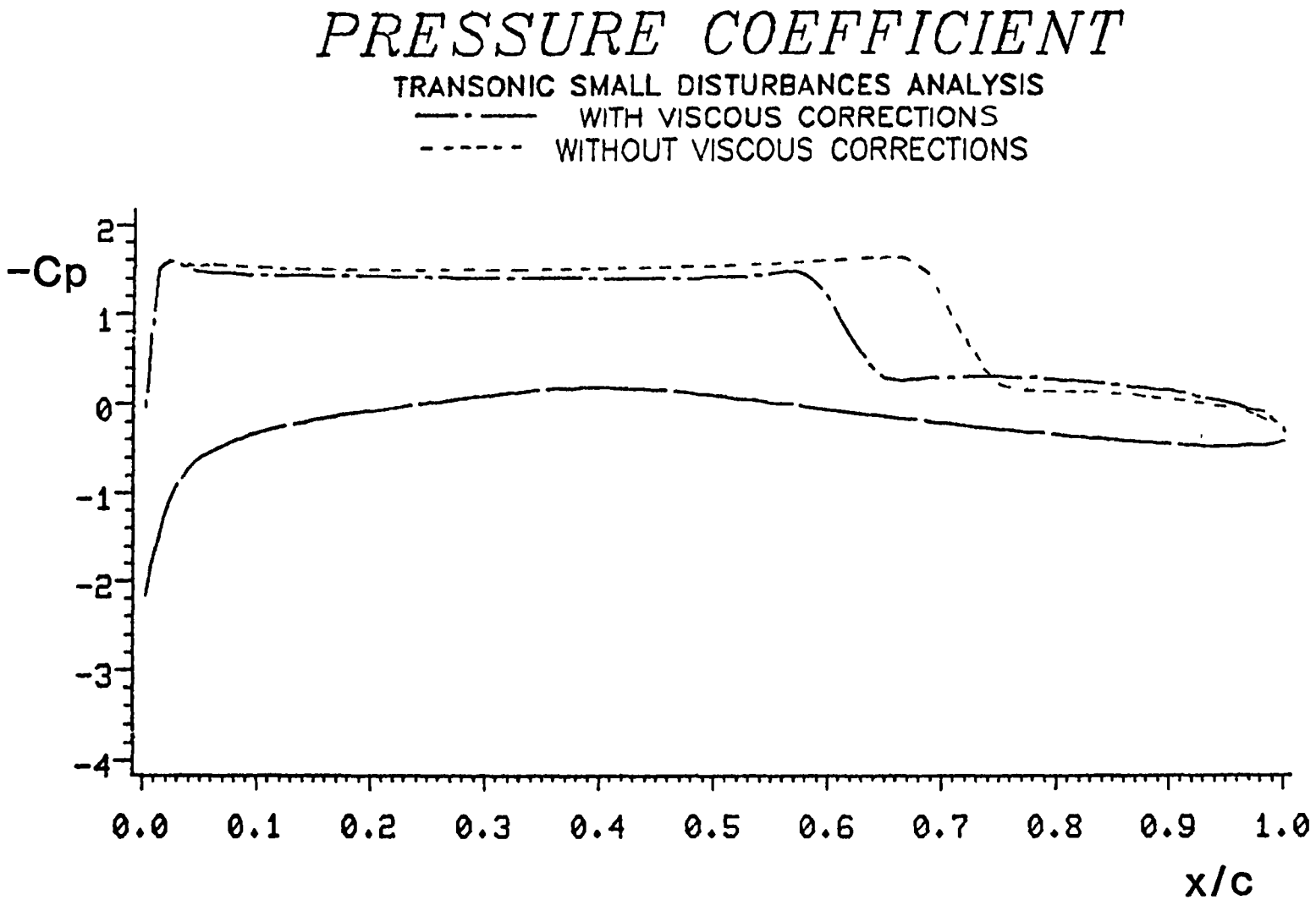

Figure 5, Pressure Coefficient (T = 39.41)

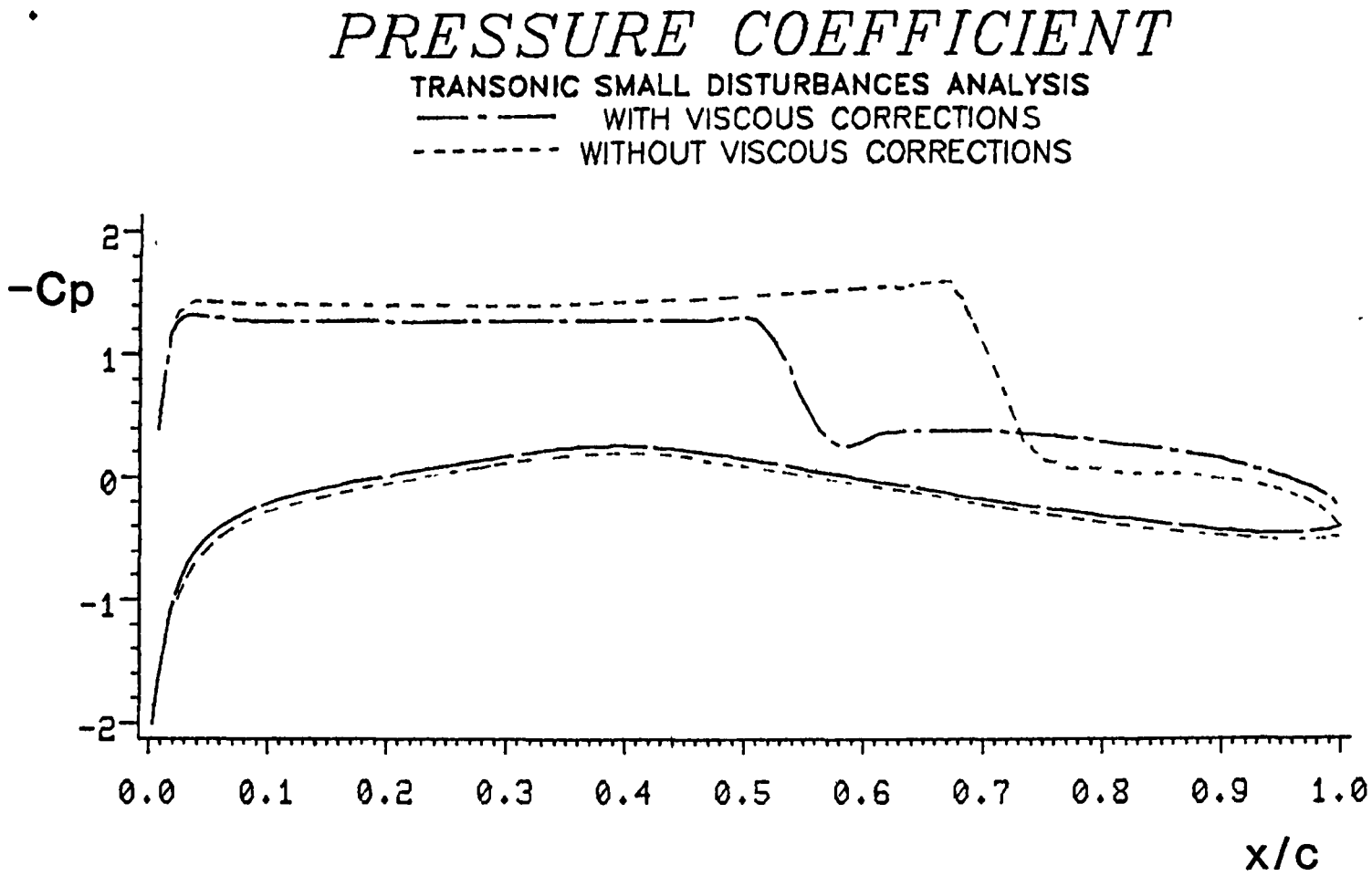

RAE 2822 AIRFOIL MINF=0.730 ALF=3.19
UNSTEADY STATE T=48.12, ALF=2.35DEG.
OSCILLATING 1.0 DEG. WITH K=0.2 AT X/C=0.5
UNSTEADY PROCEDURE FOR STEADY SOLUTION

Figure 6, Pressure Coefficient (T = 48.12)

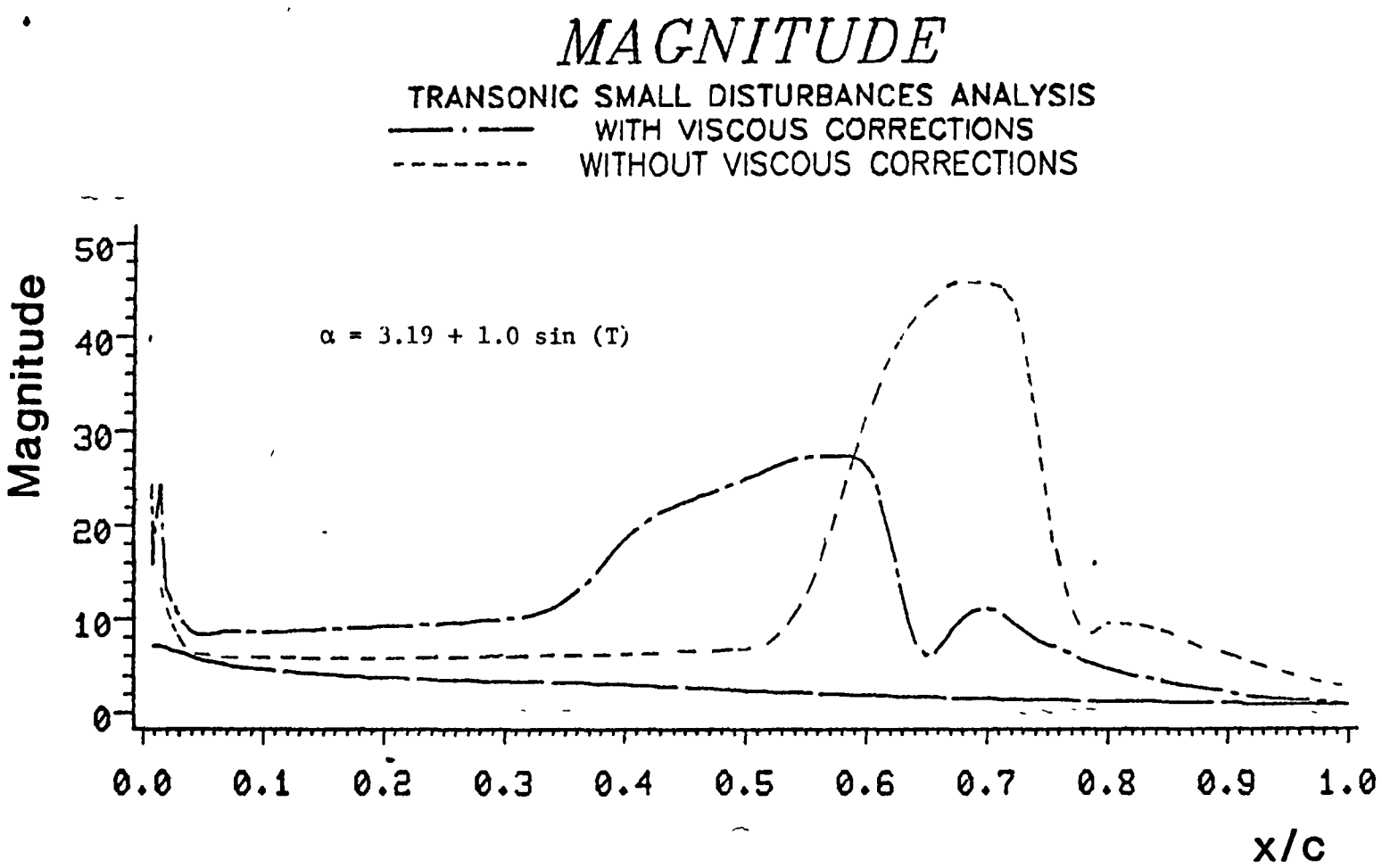

RAE 2822 AIRFOIL MINF=0.730 ALF=3.19
UNSTEADY STATE INTEGRATED RESULTS CYCLES 4-5
OSCILLATING 1.0 DEG. WITH K=0.2 AT X/C=0.5
UNSTEADY PROCEDURE FOR STEADY SOLUTION

Figure 7, Magnitude of Pressure Coefficient (RAE 2822)

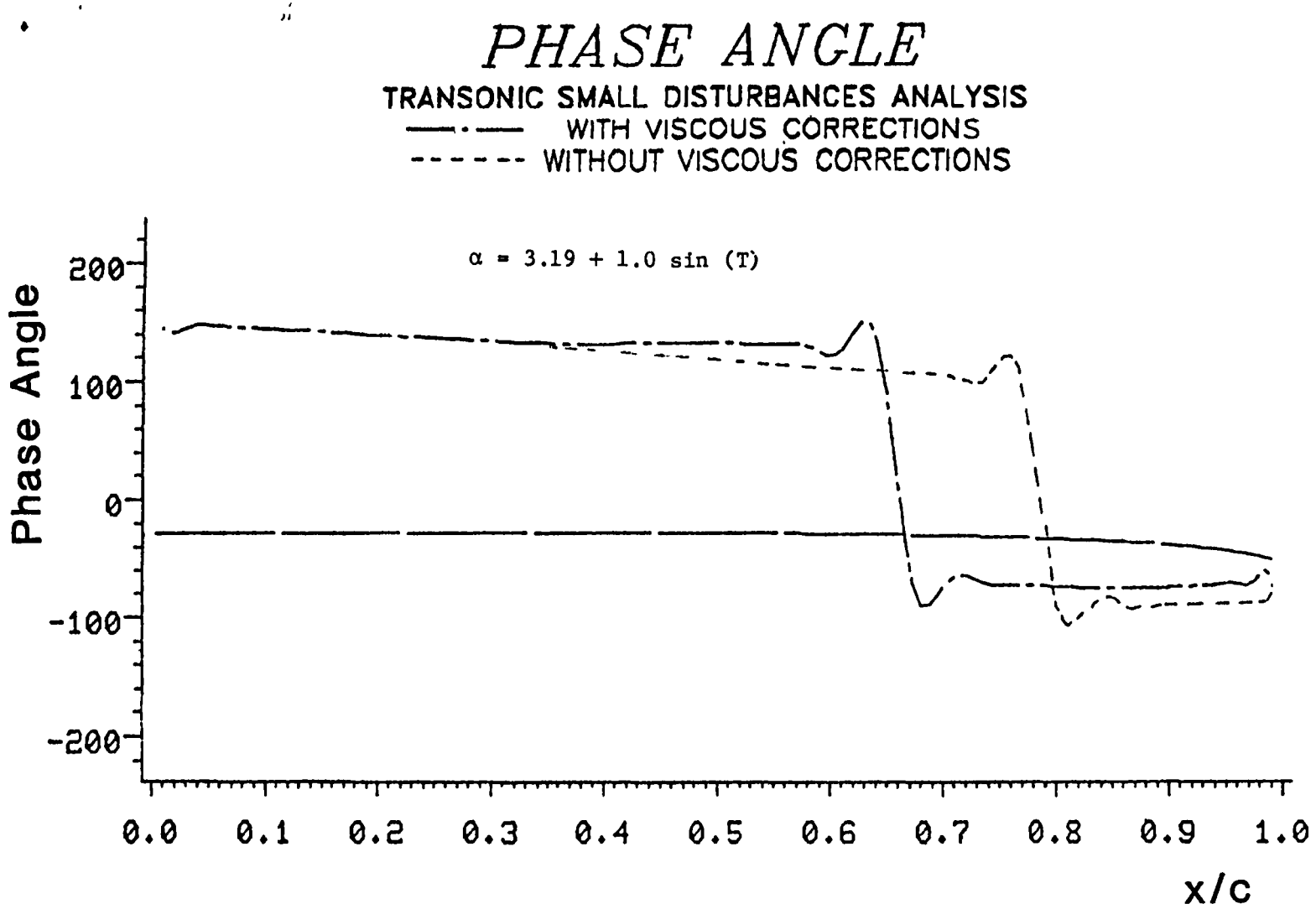

Figure 8, Phase Angle (RAE 2822)

B. NLR 7301 Airfoil

The geometry and some experimental data were given by Davis and Malcolm (28). The NLR 7301 airfoil has a maximum thickness to chord ratio of 0.1627. Due to the relatively blunt leading edge, Riegel's rule, as suggested by Rizzeta (27), was used to modify the slope of the surface contour as follows:

$$f_{xm} = f_{xo} \Big/ [1 + (f_{xo})^2]^{\frac{1}{2}} \qquad (27)$$

where f_{xm} and f_{xo} are the modified and the original slopes, respectively, several cases were analyzed. The case of $M_\infty = 0.752$, $\alpha = 0.37$ degree, $Re_\infty = 6.21 \times 10^6$ oscillating 2.10 degress about $x/c = 0.399$ at a reduced frequency $K = 0.4$ is discussed in this section.

i) Steady Solution

The standard method was used and gave converged steady state solutions. The inviscid solution took 467 iterations to converge with 324 grid points in the supersonic region. The viscous solution took 130 iterations to converge with 276 grid points in the supersonic region. Figure 9 shows the Mach number distributions. Again, the boundary layer development between the leading edge and the shock waves is responsible for the lower Mach numbers before the shock, while the wedge and the boundary layer cause the shock position to move forward. Figure 10 shows the pressure coefficient distributions in comparison with the experimental data. It can be seen that the magnitude of the pressure coefficient for the first 60% of the airfoil agrees well between the viscous solution and the experimental data. However the shock position was under-corrected with an $x/c = 0.61$ in comparison with the experimental data at an $x/c = 0.57$ and the inviscid solution at an $x/c = 0.67$. It is noted that the viscous wedge and the boundary layer models are exactly the same for both the RAE 2822 and the NLR 7301 airfoils. The reason to over-correct one and under-correct the other is not readily explainable.

ii) Unsteady Solution

Once the solution for steady state is reached, the airfoil is forced to pitch 2.01 degrees about $x/c = 0.399$ with a reduced frequency $K = 0.4$. The instantaneous angle of attack is given as follows:

$$\alpha = \alpha_o + \alpha_1 \left\{ \sin(t) + K \left[\left(\frac{x}{c}\right) - \left(\frac{x}{c}\right)_{ref} \right] \cos(t) \right\} \qquad (28)$$

where $(x/c)_{ref} = 0.399$, $\alpha_1 = 2.01$ degrees and $\alpha_o = 0.37$ degrees. The comparison between inviscid and viscous solutions are shown in Figures 11 and 12 for $\alpha = 1.95$ degrees, or $t = 21.12$, and $\alpha = 2.43$ degrees, or $T = 26.35$, respectively, It is noted that when $\alpha = 1.95$ degrees, the viscous solution gives lower pressure coefficient with shock wave moving closer to the leading edge as expected. However, when $\alpha = 2.43$ degrees, the shock location of the viscous solution is closer to the trailing edge than the inviscid solution. It appears that the viscous effect delays the response of the shock position variations when the unsteady motion is being executed at a higher frequency. The integrated results are shown in Figures 13 and 14 for the magnitude of the pressure coefficient and the phase angle, respectively. Again to avoid transient effect, the integrated results are obtained between the 4th and 5th cycles. It

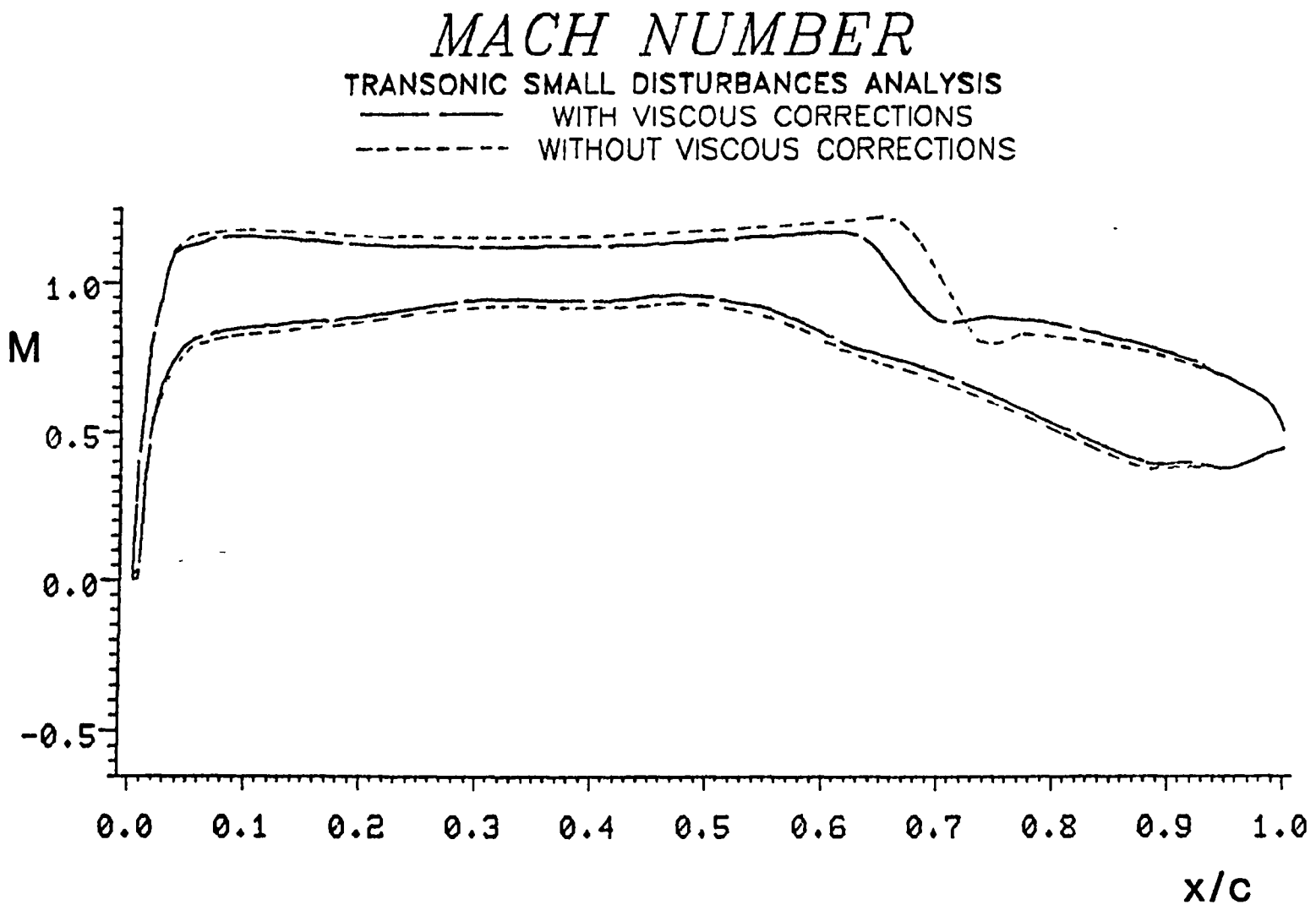

Figure 9, Mach Number Distribution, (NLR 7301)

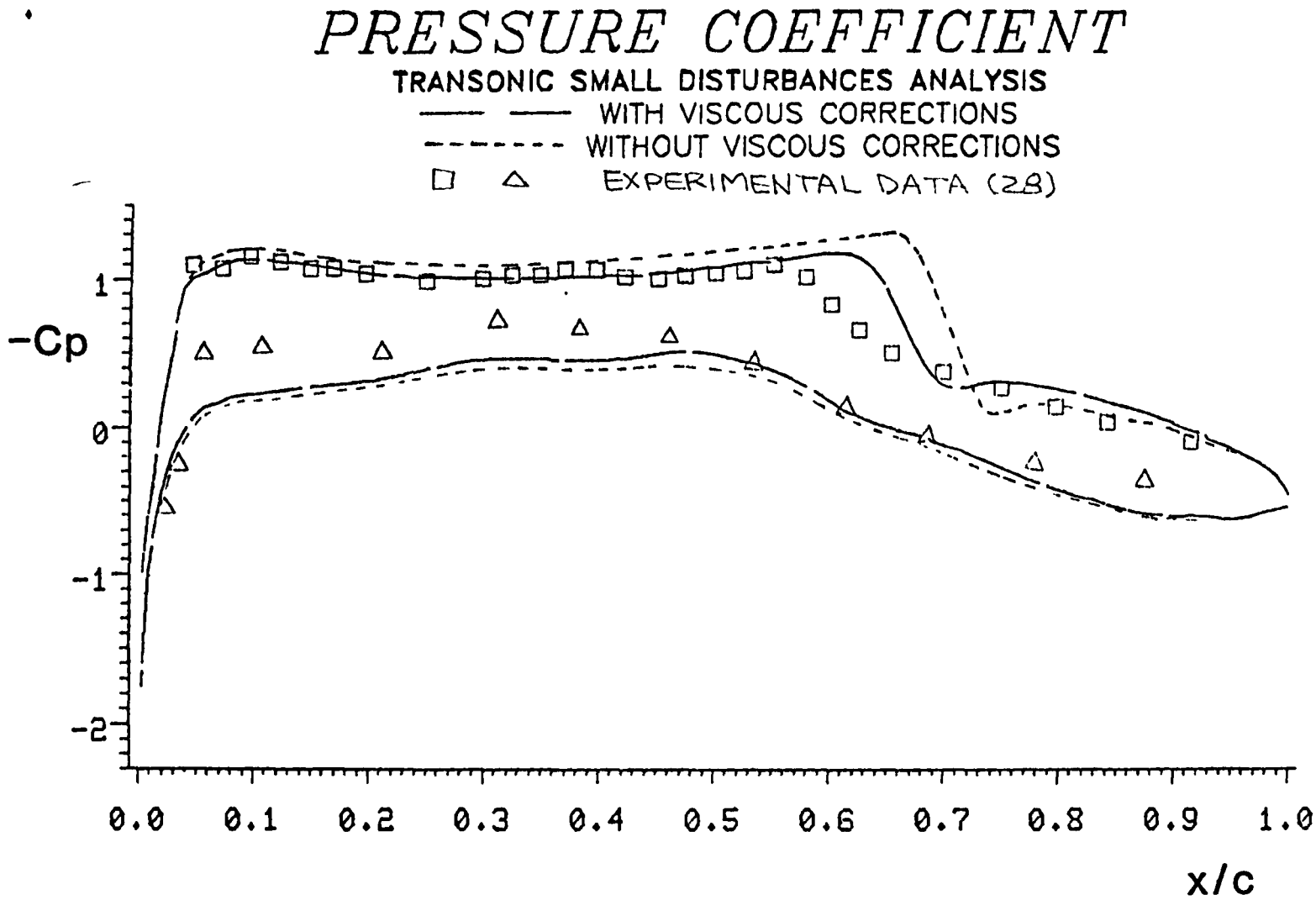

Figure 10, Pressure Distribution (NLR 7301)

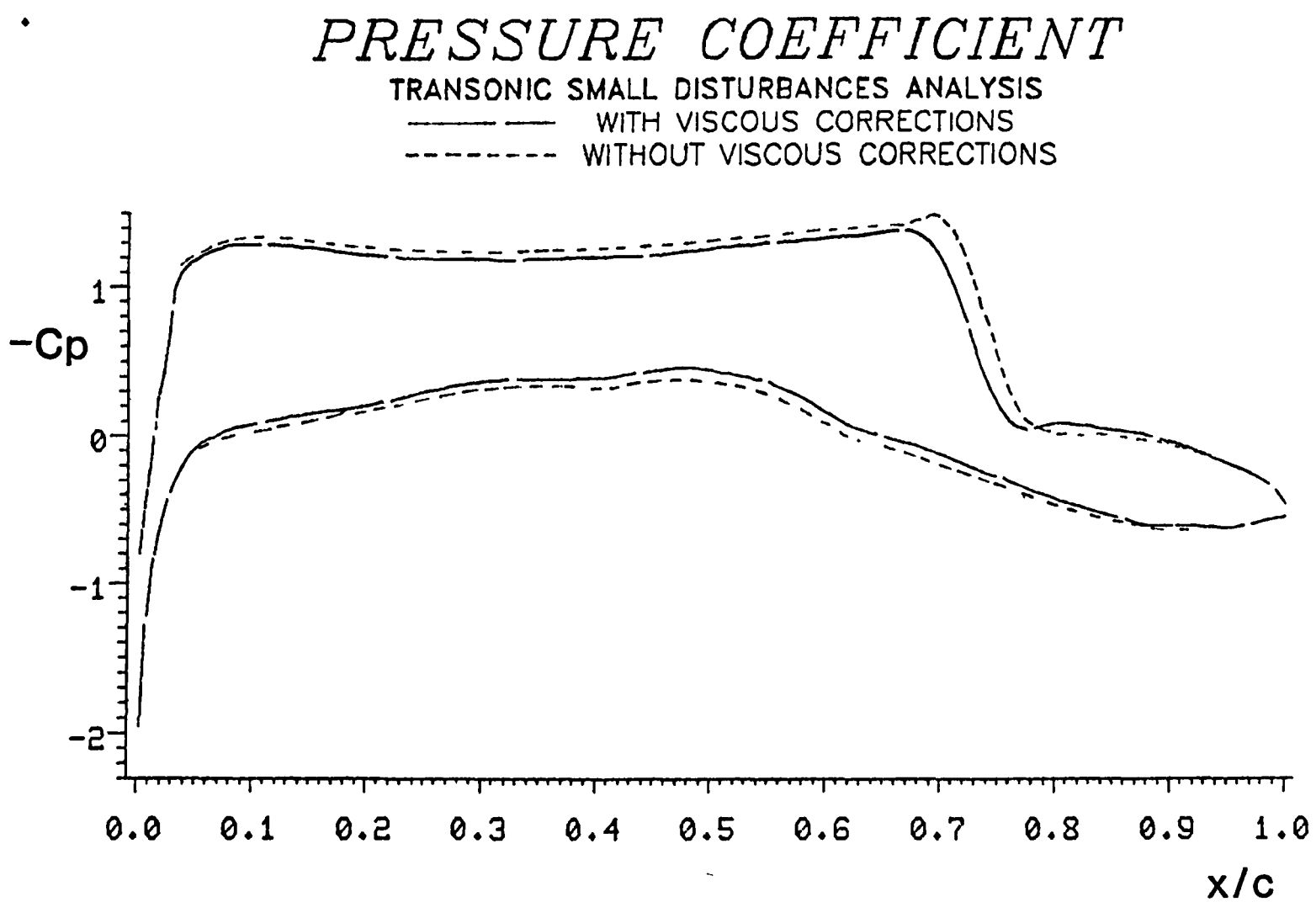

Figure 11, Pressure Coefficient (T = 21.12)

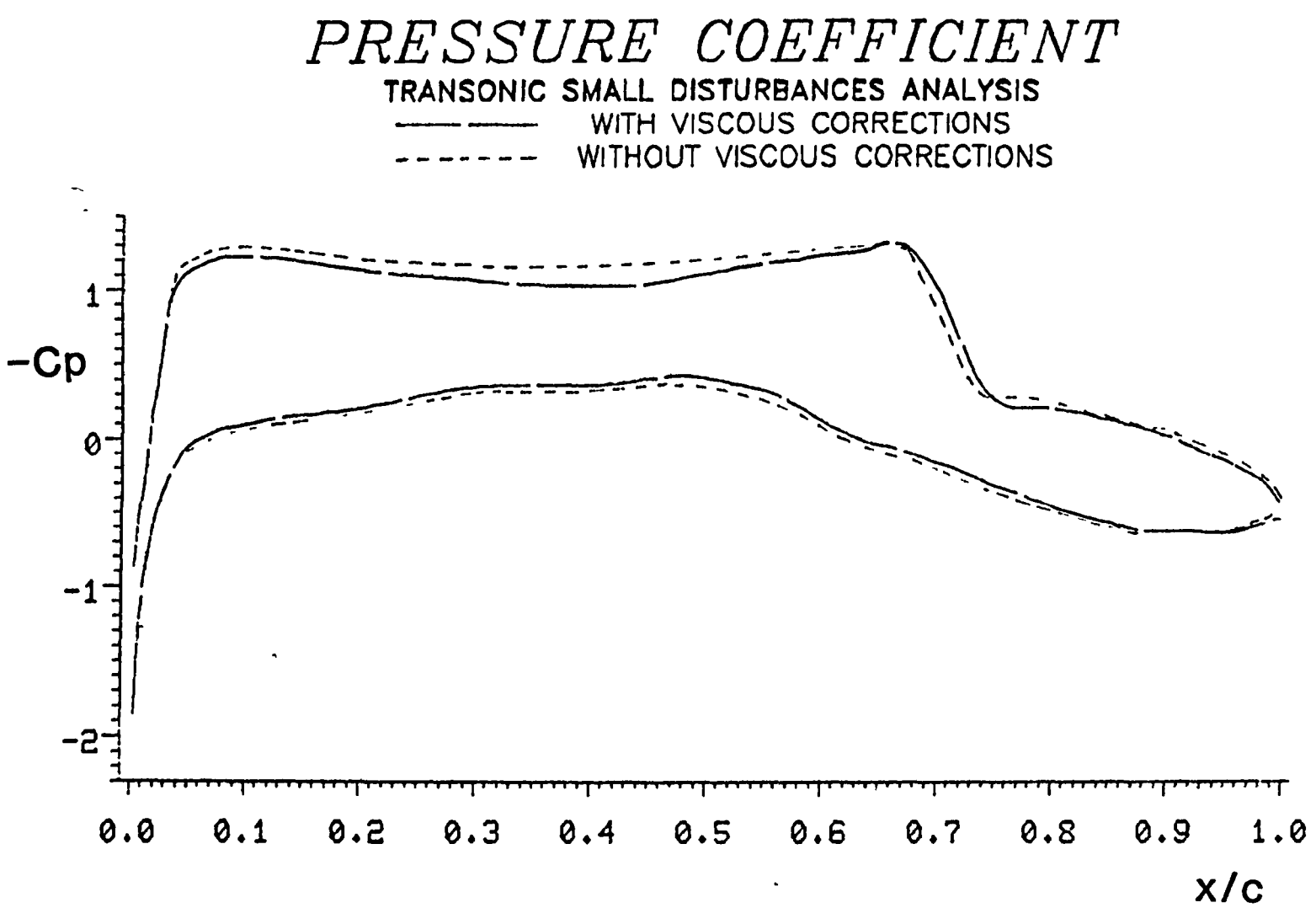

Figure 12, Pressure Coefficient (T = 26.35)

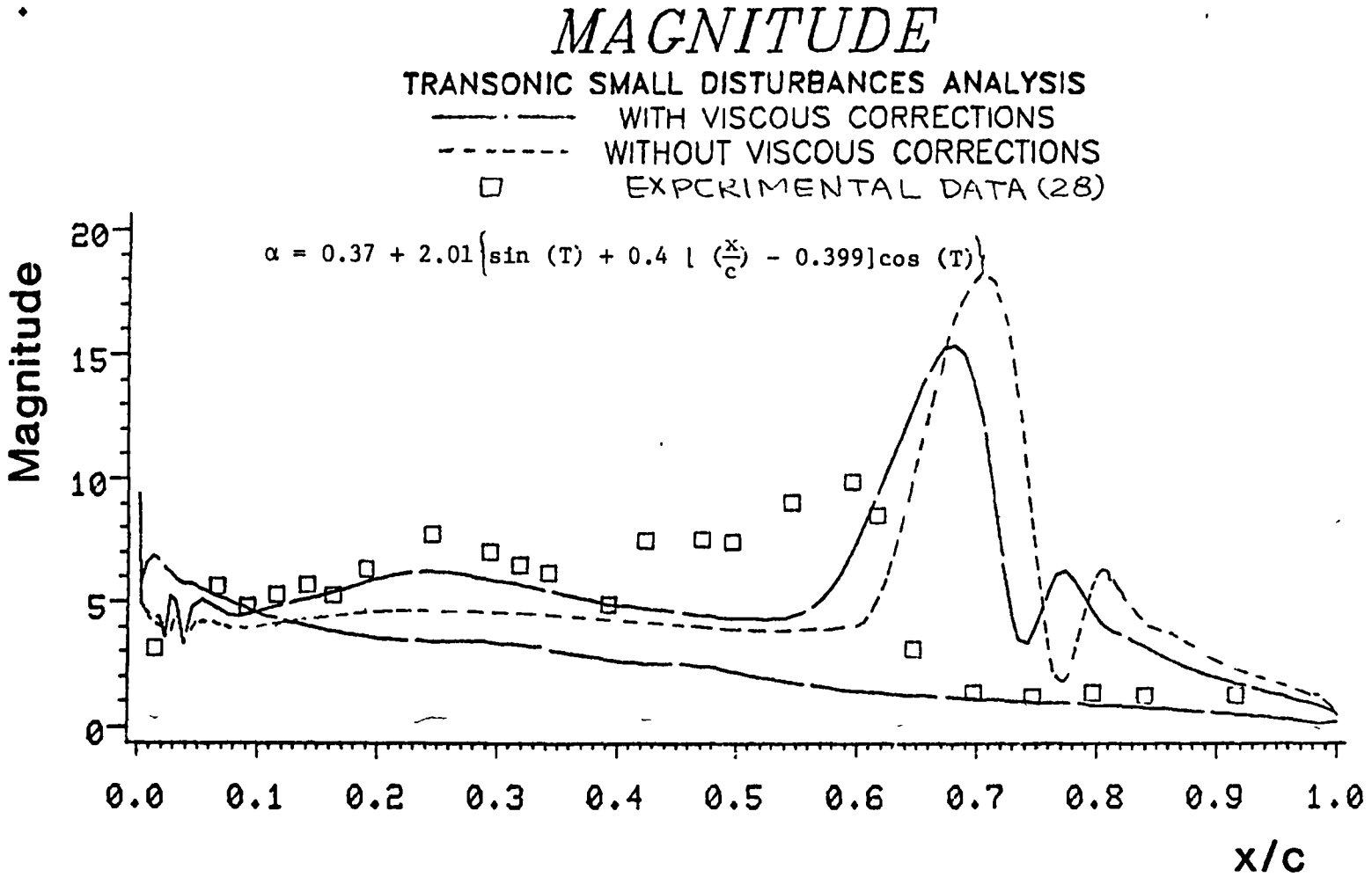

NLR 7301 AIRFOIL MINF=0.752 ALF=0.37
INTEGRATED RESULTS CYCLES 4-5
OSCILLIATING 2.01 DEG. WITH K=0.4 AT X/C=0.399
USING AF2 FOR STEADY SOLUTION

Figure 13, Magnitude of Pressure Coefficient (NLR 7301)

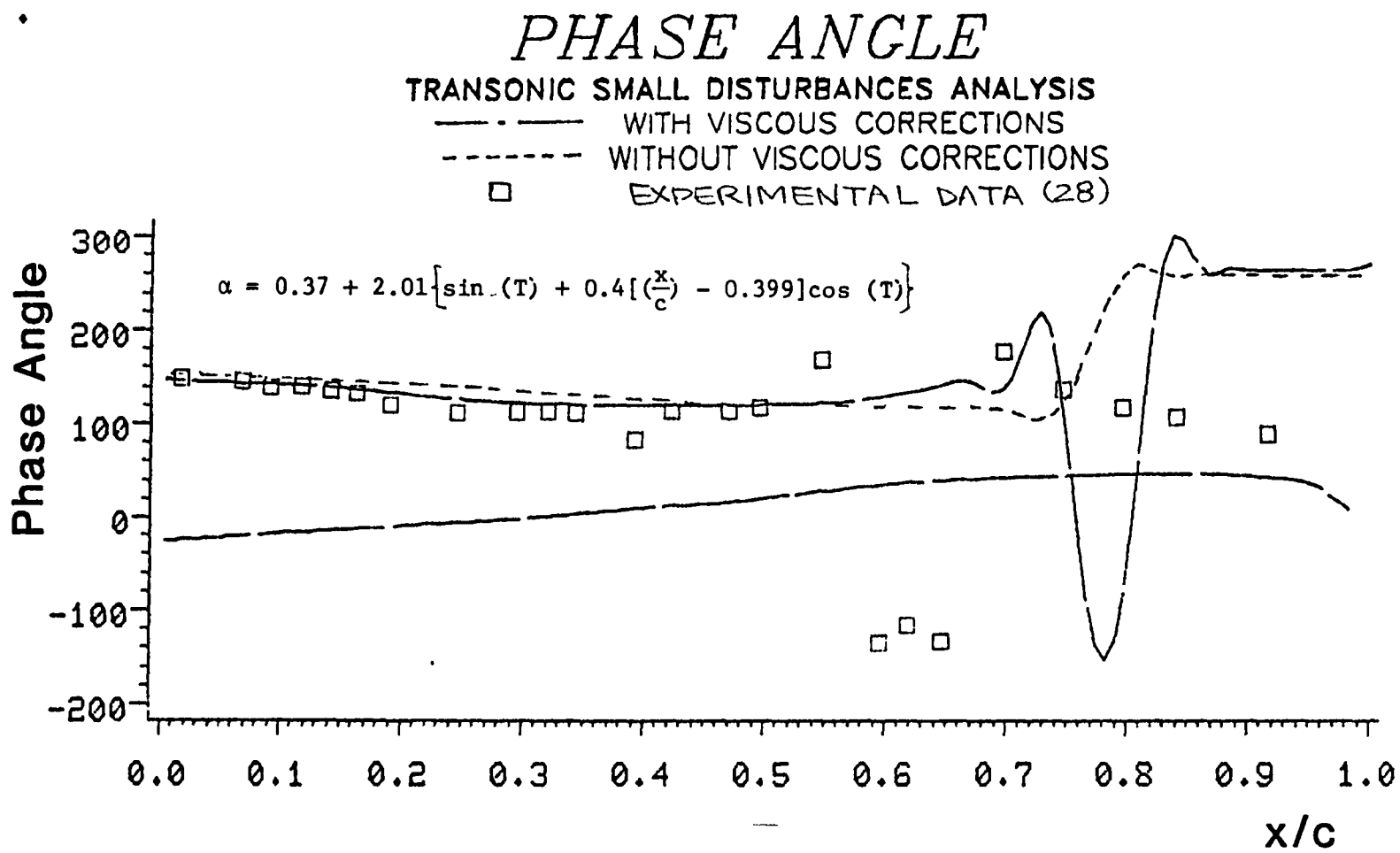

NLR 7301 AIRFOIL MINF=0.752 ALF=0.37
INTEGRATED RESULTS CYCLES 4-5
PITCHING 2.01 DEG. WITH K=0.4 AT X/C=0.399
USING AF2 FOR STEADY SOLUTION

Figure 14, Phase Angle (NLR 7301)

noted that the viscous solution gives better agreement with experimental data than the inviscid solution. Owing to the smaller number of ilterations for obtaining the steady state solution, the viscous solution uses less computational time. The CPU times were 14.85 min. for the viscous solution, and 16.87 min. for the inviscid solution on the AMDHAL 470/v7 computer. It is evident that the viscous correction not only improves the accuracy of the inviscid solution but also reduces its computational time when the standard method is used.

VI CONCLUSIONS

Modifications of the inviscid small disturbances codes LTRAN2, has been completed for considering the viscous effect on airfoils maneuvering at low frequency unsteady motions during transonic flight. Assuming the boundary layer thickness before the shock does not vary substantially due to low frequency motions, an empirical model for viscous wedge downstream of the shock can be superimposed on a displacement thickness obtained from the conventional method of solving integral boundary layer equations. The following conclusions are reached:

1. For steady state, the viscous correction requires less computational time than the inviscid solution.
2. For unsteady state, there is no noticeable increase in computational time for the viscous correction.
3. The viscous correction improved the accuracy of the inviscid solution for the sutided moderately strong shock situations.

REFERENCES

1. Spaid, F. W., and Bachalo, W. D., "Experiments on the Flow About a Supercritical Airfoil, Including Holographic Interferometry", AIAA Paper 80-0343,

2. Lin, C. L., Pepper, D. W., and Lee, S. C., "Numerical Methods for Separated Flow Solutions around a Circular Cylinder", AIAA Journal Vol. 14, 1976, pp. 900-907.

3. Chapman, D. R., "Trend and Pacing Items in Computational Aerodynamics", Seventh International Conference on Numerical Methods in Fluid Dynamics, Stanford University and NASA-Ames Research Center, June 23-27, 1980.

4. Steger, J. L., "Implicit Finite Difference Simulation of Flow About Arbitrary Geometries with Application to Airfoils", AIAA Paper 77-665, Albuquerque, New Mexico, June 27-29, 1977.

5. Ballhaus, W. F., Jameson, A., and Albert, J., "Implicit Approximate Factorization Schemes for the Efficient Solution of Steady Transonic Flow Problems", AIAA Journal, Vol. 16, No. 6, 1978 pp. 573-579.

6. Jameson, A., "Transonic Potential Flow Calculations Using Conservation Form", Proceedings AIAA Computational Fluid Dynamics Conference, June 1975, pp. 148-161.

7. "Holst, T. L., "A Fast, Conservative Algorithm for Solving the Transonic Full-Potential Equation", Proceedings AIAA 4th Computational Fluid Dynamics Conference, Williamsburg, Virginia, July 23-24, 1979, pp. 109-121.

8. Yoshihara, H. and Zonars, D., "An Analysis of Pressure Distributions on Planar Supercritical Profiles With and Without Jet Flaps at High Reynolds Numbers", GDCA-ERR-1964, December 1971.

9. Nash, J. and Scruggs, R, "An Automated Procedure For Computing the Three-Dimensional Transonic Flow over Wing Body Combinations, Including Viscous Effect", AFFDL-TR77-122, Vol. III, Grumman Aerospace Corporation, October 1977.

10. "Green, J. E. Weeks, D. J., and Brooman, J. N. F., "Prediction of Turbulent Boundary Layers and Wakes in Compressible Flow by a Lag-Entrainment Method", Report Memoranda 3791, Royal Aeronautical Establishment, England, 1977.

11. Collyer, M. R. and Lock, R. C., "Prediction of Viscous Effects in Steady Tronsonic Flow Past an Aerofoil", Aeronautical Quarterly, Vol. XXX, August 1979.

12. Melnik, R. E., Chow, R. R., Mead, H. R. and Jameson, A., "An Improved Viscid/Inviscid Interaction Procedure for Transonic Flow over Airfoils", NASI-12426, Grumman Aerospace Corporation, February 1980.

13. Jameson, A., "Numerical Computation of Transonic Flow with Shock Waves", Symposium Transonicum II, Springer-Verlag, New York, 1975.

14. Jameson, A., "Acceleration of Transonic Potential Flow Calculations on Arbitrary Mesles by Multiple Grid Method", Proceedings AIAA computational Fluid Dynamic Conference, July 1979, pp. 122-146.

15. Lee, S. C., and Van Dalsam, W. R., "Numerical Simulation of Steady Transonic Flow About Airfoils", Proceedings AIAA Computational Fluid Dynamics Conference, 1980, pp. 69-76.

16. "Dougherty, F. C., Holst, T. L., Grundy, K. L., and Thomas, S. D., "TAIR - A Transonic Airfoil Analysis Computer Code", NASA TM 81296, 1981.

17. Ballhaus, W. F. and Goorjian, P. M., "Implicit Finite-Difference Computation of Unsteady Transonic Flows About Airfoils", AIAA Journal, Vol. 15, No. 12, 1977, pp. 1728-1735.

18. Rizzetta, D. P., and Yoshihara, H. "Computations of the Pitching Oscillation of a NACA 64A010 Airfoil in the Small Disturbance Limit", AIAA Paper 80-0128, Pasadena, Calif. January 14-16, 1980.

19. Hessenius, K. A. and Goorjian, P. M., "A Validation of LTRAN2 with High Frequency Extension by Comparisons with Experimental Measurements of Unsteady Transonic Flows", TM 81307, NASA, July 1981.

20. Landahl, M, "Unsteady Transonic Flow", Pergamon Press, New York, 1961.

21. Cohen, C. B. and Reshotko, E., "The Compressible Boundary Layer with Heat Transfer and Arbitrary Pressure Gradient", NACA TR-1294, 1956.

22. Sasman, P, K. and Cresci, R. J., "Compressible Turbulent Boundary Layer with Pressure Gradient and Heat Transfer", AIAA Journal, Vol. 4, No. 1, 1966, pp. 19-25.

23. Mager, A., "Transformation of the Compressible Turbulent Boundary Layer", Journal of Aerospace Science, Vol. 25, No. 5, 1958, pp. 305-311.

24. Tetervin, N., "The Application of the Reference-Enthalpy Method to Friction Formulas", Journal of Aerospace Science, Vol. 29, 1962, p. 493.

25. McNally, W. D., "FORTRAN Program for Calculating Compressible Laminar and Turbulent Boundary Layers in Arbitrary Pressure Gradients", NASA TN D-5681, 1970.

26. Cook, P. H., McDonald, M. A. and Firman, M.C.P., "Aerofoil RAE 2822 Pressure Distributions and Boundary Layer and Wake Measurements", AGARG-AR-138.

27. Davis, S. S. and Malcolm, G. N., "Experimental Unsteady Aerodynamics of Conventional and Supercritical Airfoils", NASA TM 81221, August 1980.

28. Rizzeta, D. P. "Procedures for the Computation of Unsteady Transonic Flows Including Viscous Effects", NAS2-10762, The Boeing Company, August 1981.

1 Report No	2 Government Accession No	3 Recipient's Catalog No
NASA CR-166335		

4 Title and Subtitle	5 Report Date
Viscous Effect on Airfoils for Unsteady Transonic Flows	June 1982
	6 Performing Organization Code
7 Author(s)	8 Performing Organization Report No
Shen C. Lee	
9 Performing Organization Name and Address	10 Work Unit No
University of Missouri (Rolla) Rolla, Missouri 65401	T4211
	11 Contract or Grant No
	NCA2-OR450-001
12 Sponsoring Agency Name and Address	13 Type of Report and Period Covered
National Aeronautics and Space Administration Washington, DC 20546	Contractor Report Final Report
	14 Sponsoring Agency Code
	505-31-11

15 Supplementary Notes

Technical Monitor: Terry L. Holst, MS 202A-14 (415) 965-6415
NASA Ames Research Center FTS 448-6415
Moffett Field, CA 94035

16 Abstract

This study considers the viscous effect on aerodynamic performance of an arbitrary airfoil executing low frequency maneuvers during transonic flight. Modification of the small disturbance code, LTRAN2, was made by using a conventional integral method, BLAYER, for the boundary layer and an empirical relation, viscous wedge, for simulating the suddenly thickened boundary layer behind the shock. Before the shock, only the boundary layer displacement thickness was evaluated. After the shock the empirical wedge thickness was superimposed on the boundary layer thickness along the surface as well as in the wake region. The pressure coefficients were calculated for both steady and unsteady states. The viscous solution takes fewer iterations to obtain the converged steady state solution. Comparisons were made with experimental data and the inviscid solution. The viscous solution agrees better with the experimental data with about the same (or slightly less) amount of computational time.

17 Key Words (Suggested by Author(s))	18 Distribution Statement
Unsteady Transonic Flow Computational Methods Boundary Layers	Unlimited Star Category - 02

19 Security Classif (of this report)	20 Security Classif (of this page)	21 No of Pages	22 Price*
Unclassified	Unclassified	37	

*For sale by the National Technical Information Service, Springfield, Virginia 22161

End of Document